Origin and Sustainability of The Population of Asteroids Captured in the Exterior Resonance 1:2 with Mars

Tabaré Gallardo[a,*], Julia Venturini[a], Fernando Roig[b], Ricardo Gil-Hutton[c]

[a] *Departamento de Astronomía, Instituto de Física, Facultad de Ciencias, Iguá 4225, 11400 Montevideo, Uruguay*

[b] *Observatório Nacional, Rua General José Cristino 77, 20921-400, Rio de Janeiro, Brasil*

[c] *Complejo Astronómico El Leoncito (CASLEO), Av. España 1512 sur, J5402DSP San Juan, Argentina*

Abstract

At present, approximately 1500 asteroids are known to evolve inside or sticked to the exterior 1:2 resonance with Mars at $a \simeq 2.418$ AU, being (142) Polana the largest member of this group. The effect of the forced secular modes superposed to the resonance gives rise to a complex dynamical evolution. Chaotic diffusion, collisions, close encounters with massive asteroids and mainly orbital migration due to the Yarkovsky effect generate continuous captures to and losses from the resonance, with a fraction of asteroids remaining captured over long time scales and generating a concentration in the semimajor axis distribution that exceeds by 20% the population of background asteroids. The Yarkovsky effect induces different dynamics according to the asteroid size, producing an excess of small asteroids inside the resonance. The evolution in the resonance generates a signature on the orbits, mainly in eccentricity, that depends on the time the asteroid remains captured inside the resonance and on the magnitude of the Yarkovsky effect. The greater the asteroids, the larger the time they remain captured in the resonance, allowing greater diffusion in eccentricity and inclination. The resonance generates a discontinuity and mixing in the space of proper elements producing misidentification of dynamical family members, mainly for Vesta

*Corresponding author

Email address: gallardo@fisica.edu.uy (Tabaré Gallardo)

and Nysa-Polana families. The half-life of resonant asteroids large enough for not being affected by the Yarkovsky effect is about 1 Gyr. From the point of view of taxonomic classes, the resonant population does not differ from the background population and the excess of small asteroids is confirmed.

Keywords: Asteroids, dynamics, Asteroid Vesta, Resonances, orbital, Rotational dynamics

1. Introduction

The asteroid Main Belt is sculpted by mean motion resonances (MMR), mainly with Jupiter, and secular resonances with the giant planets. However, there are also relatively strong exterior MMR with the terrestrial planets, especially in the inner region of the Belt (Gallardo, 2006). For any terrestrial planet, its exterior 1:2 MMR is the strongest one, and in the case of Mars, this resonance (1:2M) is located in the inner main belt at $a \sim 2.4184$ AU. This MMR produces an evident concentration of asteroids in semimajor axis (Gallardo, 2007). How was this concentration created? How long does an asteroid stay in resonant motion? Is there any mechanism that replenishes the population? The study of the dynamics of the 1:2M resonance and the origin and evolutionary paths of their members is the aim of this paper.

If we try to approximate the perturbing function for this resonance by an analytical approach using a series of terms of different orders in the small parameters e and i, the lowest order terms depend on the critical angles $\sigma = 2\lambda - \lambda_M - \varpi$ and $\sigma_1 = 2\lambda - \lambda_M - \varpi_M$, where subscript $_M$ refers to Mars. These terms are the ones that are usually librating in the case of asteroids located in the resonance. The first one is factorized by the asteroid's eccentricity, e, and the second one is factorized by Mars' eccentricity, e_M. Higher order terms, and consequently dynamically less important ones, depend on other combinations of $\lambda, \varpi, \Omega, \lambda_M, \varpi_M$ and Ω_M, which define other critical angles. In very particular cases, these critical angles can librate too.

In this resonance, as in any exterior resonances of the type 1:N, the librations of the critical angle σ occur around central values, σ_c, that depend on the eccentricity, giving rise to the so-called "asymmetric librations" because they do not occur around 0^o or 180^o as is usual in other MMRs. The angles σ and σ_1, and especially the first one, are the most important indicators of the resonant state but not the only ones. In particular, the libration theory predicts an oscillation of the osculating semimajor axis around a mean, a_m,

or "proper" value, a_p, which is characteristic of the resonance. The difference between a_m and a_p is that the first one is the mean over some time span and the latter is obtained from a frequency analysis. Moreover, it is known that the resonance width, i.e. the region in semimajor axis where the resonant motion dominates, is proportional to the orbital eccentricity defining a region in the (a, e) space where the resonance drives the orbital evolution.

Approximately 1500 asteroids are performing librations, horseshoes and transitions between both asymmetric libration centers, which are the typical trajectories in this resonance. About 400 of these asteroids librate around the asymmetric libration centers with amplitudes $\Delta\sigma = \sigma_{max} - \sigma_{min} < 180°$. The states of the resonant population now and after 1 Myr of orbital evolution are shown in Figs. 1 and 2 of Gallardo (2009). Asteroids change their libration center and change between librations and horseshoe trajectories, but the number of asteroids with asymmetric librations and horseshoes is similar at the beginning and at the end of this time-span. Therefore, we may conclude that the population is in equilibrium over such timescale. Table 1 lists the resonant asteroids with absolute magnitude $H < 14$. The evolution of the critical angle and eccentricity of (142) Polana is shown in Fig. 1. Proper elements shown in the table were derived from our numerical study which is explained in Section 2, and the complete list can be found at `http://www.fisica.edu.uy/~gallardo/marte12/all.html`. In some cases, normally at low e, the libration amplitude of σ_1 is smaller than the libration amplitude of σ.

At variance to the resonances with Jupiter that dominate the time evolution of the asteroid eccentricity, the libration theory predicts that the eccentricity is almost unaffected by the 1:2M resonance, but its evolution is dominated by the secular forced modes on the asteroid orbit generated by the planetary system. In fact, the variations in eccentricity shown in Fig. 1 are due to a secular evolution, not to the libration itself. These important oscillations in the eccentricity affect the locations of the libration center and the amplitude of the asymmetric librations of the critical angle (Fig. 2 from Gallardo, 2007). Nevertheless, these are long term periodic oscillations and they do not destroy the resonant motion. This can be checked by following the time evolution of a_p or a_m, which remain locked in the resonance's domain. However, the irregular evolution of σ no longer guarantees the resonant protection mechanism against close encounters with Mars, allowing such close encounters for high eccentricity orbits.

The region around the location of the resonance is occupied by the dynam-

Asteriod	H	e_p	$i_p[^\circ]$	$\sigma_c[^\circ]$	$\Delta\sigma[^\circ]$
(142) Polana	10.2	0.1573	3.198	105	211
(1998) Titius	12.2	0.0848	7.764	70	124
(3665) Fitzgerald	12.6	0.1151	9.557	289	95
(9652) 1996 AF2	13.0	0.1967	6.860	96	125
(2798) Vergilius	13.1	0.0438	5.944	214	200
(11576) 1994 CL	13.3	0.1394	11.111	80	131
(11055) Honduras	13.5	0.1937	11.774	70	72
(11751) 1999 NK37	13.7	0.1347	2.656	94	142
(8748) 1998 FV113	13.7	0.0917	5.937	226	170
(42786) 1998 WU4	13.8	0.1196	22.383	141	197
(2994) Flynn	13.9	0.1974	2.649	275	102

Table 1: The largest resonant asteroids with critical angles (σ) showing asymmetric librations (libration center $\sigma_c \neq 0^\circ, 180^\circ$) or transitions between libration centers. H is the absolute magnitude, e_p and i_p are proper eccentricity and inclination, and $\Delta\sigma = \sigma_{\max} - \sigma_{\min}$.

ical families of Vesta, Massalia and the Nysa-Polana complex (Cellino et al., 2001; Mothé Diniz et al., 2005; Zappalà et al., 1995). The 1:2M resonance generates some dynamical signatures to the Massalia family (Vokrouhlický et al., 2006), and should generate some dynamical signatures to the other families, a topic that we will explore in this paper.

The resonance is very narrow in semimajor axis units, but even so it generates a feature in the distribution of main belt asteroids, which means that it is strong enough to affect their dynamical evolution. We are interested in determining the resonance ability to retain asteroids in spite of the chaotic diffusion, the Yarkovsky effect, and the mutual collisions and close encounters with massive asteroids that may occur in that region.

2. Resonant population: dynamical and physical properties

We have explored the dynamics of the resonance by a series of numerical integrations using the integrator EVORB (Fernández et al., 2002). Our model includes the planets from Venus to Neptune, ignoring the planet Mercury, plus real and fictitious populations of asteroids. The orbital elements were taken from the ASTORB database (`ftp://ftp.lowell.edu/pub/elgb/astorb.html`) and the output of the integrations was analyzed using fourier techniques (Gallardo and Ferraz-Mello, 1997). The numerical integrator is basically a

leapfrog scheeme with time step of 0.02 yr in the absence of close encounters, which switches to a Bulirsch-Stoer routine in the case of close encounters of the asteroids with the planets. We also analyzed the physical properties of the asteroids, like absolute magnitude, H, surface colors from the Sloan Digital Sky Survey Moving Objects Catalogue (SDSS-MOC) photometry, and membership to the known dynamical families in this region.

2.1. Resonance dynamics

In order to find the properties of the resonant motion, we looked for known asteroids with osculating semimajor axes near the resonant value and follow their orbital evolution by means of numerical integrations. We started our analysis by integrating 4022 orbits from the ASTORB file with $2.416 \leq a \leq 2.422$ AU. The resonance domain in semimajor axis can be visualized in several ways. For example, in Fig. 2, we show a plot of a_p versus the principal frequency associated with the time evolution of a. Both values were deduced automatically from the spectral analysis of the time evolution of a and σ over 30×10^3 years. We define a_p as the time-independent term in the fourier series expansion of the osculating $a(t)$. In Fig. 2, the central feature at $a_p \simeq 2.4184$ AU corresponds to asteroids performing librations with periods going from 2,500 to 10,000 yr. The two inclined lines at both sides of the central feature are due to asteroids with their critical angles performing circulations. Moving in a_p from the left (where $d\sigma/dt > 0$) to the right, the circulation frequency diminishes up to the point where $d\sigma/dt \sim 0$, and the librations start generating the discontinuity in a_p which accumulates at $a_p \simeq 2.4184$. Continuing to the right we find, again, the circulation of the critical angle but in this case with $d\sigma/dt < 0$ and with increasing frequency. Between the central feature and the inclined lines, there are two regions where transitions between circulation and libration are observed. For example, an asteroid with $a_p = 2.416$ shows only circulation in the critical angle, but this circulation frequency is evident in the time evolution of a, which means that there are traces of the resonance in its dynamical evolution. No frequencies associated with σ were found for $a_p < 2.414$ and $a_p > 2.423$, so no dynamical traces of the resonance can be expected there.

Performing a spectral analysis of the variables ($k = e\cos\varpi$, $h = e\sin\varpi$) and ($p = i\cos\Omega$, $q = i\sin\Omega$) over 1 Myr of numerical integration, it was possible to determine the forced and proper modes in the evolution of e and i. Forced modes are the oscillation modes corresponding to the fundamental frequencies of the planetary system, and proper modes are the oscillation

modes with large amplitudes and frequencies different from the fundamental ones (Murray and Dermott, 1999). We call e_p and i_p the amplitudes of the forced modes. Contrary to Fig. 2, where we cannot distinguish between different eccentricities, Fig. 3 shows the structure of the resonance with increasing width at higher e_p, and the huge concentration of asteroids at $2.4180 < a_p < 2.4188$, with two deep gaps at both sides of the central peak. An analogous plot using synthetic proper elements from AstDyS (`http://hamilton.dm.unipi.it/astdys/`) looks very similar to our Fig. 3. Considering the peak and the gaps, there is an excess of asteroids in the region $2.416 < a_p < 2.421$. According to the AstDyS database, that only includes asteroids with well determined orbits so it should be less biased than our sample, we estimate that in a range of $\Delta a_p \simeq 0.005$ AU there are approximately 1900 asteroids in the domain of the resonance, against approximately 1600 asteroids that are far from the resonance (background). Therefore, in that database, there is an excess of approximately 300 resonant asteroids, which means that the resonance generates a population excess of 20% over the background.

Figures 2 and 3 can be used to define the limits where the resonance is dominant over the other periodic terms that affect the time evolution of the asteroid semimajor axis. However, the best indicator of these limits appears in Fig. 4, that was obtained by plotting the 1 Myr averages of the orbital elements of 100 resonant asteroids from the ASTORB file evolving over 1 Gyr. The concentration at the borders of the resonance is due to the phenomenon of "resonance stickiness" (Malishkin and Tremaine, 1999), and the behavior at $e_m > 0.2$ is due to the overlap of resonances that cause a strong chaotic diffusion (Morbidelli and Nesvorný, 1999).

The fundamental frequencies g_5 and g_6 are clearly present in the secular evolution of the eccentricity, and f_6 appears in the inclination. The proper elements e_p and i_p are concentrated around some values, indicating their relation to particular collisional families (Fig. 5).

2.2. Physical properties

According to the orbital evolution over 1 Myr, we defined a subsample of asteroids clearly captured in the resonance ($2.4180 < a_p < 2.4188$) and a subsample of asteroids clearly outside of both sides of the resonance ($a_p < 2.4154$ and $a_p > 2.4214$). In order to determine the fraction of these bodies that belong to asteroid dynamical families, we applied the Hierarchical Clustering Method (following the procedure described in Mothé Diniz et al., 2005) to

Family	a_p[AU]	e_p	i_p[°]	% of R	% of NR
Vesta	2.25 - 2.48	0.08 - 0.12	5.7 - 7.5	2.9	6.2
Nysa-Polana	2.32 - 2.47	0.14 - 0.20	2.0 - 3.2	5.3	9
Massalia	2.36 - 2.46	0.15 - 0.17	1.3 - 1.7	3.3	3.7

Table 2: Percentage of dynamical family members in the subsample of resonant asteroids (R) and in the subsample of non resonant asteroids (NR). There is a deficiency of identified family members inside the resonance.

the AstDyS catalog of analytical proper elements, and identified the major asteroid families in the neighborhood of the 1:2M resonance. We found that only 11.5% of the clearly resonant asteroids belong to the dynamical families of either Vesta, Nysa-Polana or Massalia. For the non resonant subsample, only 18.9% are members of any of the above families (see details in Table 2). The families of Vesta and Nysa-Polana clearly have less members inside the resonance than outside. Results for Nysa-Polana family are consistent with Fig. 26 of Morbidelli et al. (1995), where a decrease in the density number of the family members is observed at $a \simeq 2.42$. As we will show later, the lack of family members in the resonance is related to the diffusion in (e, i) that hinders the identification of family members (Vokrouhlický et al., 2006; Carruba and Michtchenko, 2009).

For both resonant and non resonant groups, we analyzed the distribution of asteroids' surface colors using the photometric data from Sloan Digital Sky Survey (SDSS). We did not find any remarkable differences between the groups, which led us to conclude that the resonance is not dominated by any particular asteroid taxonomic class. The analysis of the absolute magnitude (H) distribution confirmed a tendency to higher H (smaller asteroids) for the resonant population (Gallardo, 2007). However, the resonant population is more eccentric, on average, than the non resonant one (Fig. 6), and this might favor the discovery of smaller asteroids inside the resonance than outside. To correct this bias, we analyzed the H distribution of two samples of 855 asteroids each, one from the resonant population and the other from the non-resonant population, having the same eccentricity distribution in the range $0 < e < 0.25$ (Fig. 7). Using a Kolmogorov-Smirnov test for cumulative distributions (Press et al., 1997), we found that both samples have different H distributions with a level of confidence of 98.7%, and that small asteroids are more abundant in the resonant sample. We will discuss this point later in Section 3.

2.3. Long term evolution of the resonant population

We integrated numerically 100 real asteroids over 1 Gyr, and calculated the mean eccentricity and the mean semi-major axis over intervals of 1 Myr. Then, using the limits of the 1:2M resonance defined by Fig. 4, we determined the number of asteroids captured in the resonance at each instant and the result is shown in Fig. 8. By fitting this data to an exponentially decaying function, we can deduce a half-life of ~ 2.5 Gyr. This value will be revised later in Section 3.

While evolving inside the resonance, the asteroids exhibit a diffusion mainly in e_m, but also in i_m, which in general is roughly proportional to the lifetime in the resonance. A typical variation in e_m is about 0.05 after some hundred million years of evolution inside the resonance, but some asteroids may exhibit larger changes in e_m, and variations up to 0.15 can be achieved for the asteroids that remain captured over 1 Gyr. We have also found that the larger proper inclination, the larger the diffusion in e_m and i_m. For example, for $i_p = 1.5°$, typical of the Massalia family, the diffusion in eccentricity is 0.05 and in inclination is 1.2°, whereas for $i_p = 6.6°$, typical of the Vesta family, the diffusion in eccentricity is 0.08 and in inclination is 1.6°. The success in the identification of resonant members of the Massalia family, in comparison to the members of the Nysa-Polana family, could be explained partially because of their low proper inclination and, in consequence, their lower diffusion in eccentricity and inclination. Figure 9 shows the evolution in (e_m, i_m) for the complete sample. When e_m crosses the value ~ 0.22, the diffusion in a_m and i_m increases and the asteroids evolve in a chaotic region generated by the overlap of several resonances, eventually leaving the 1:2M resonance.

In our simulation, the first asteroid had a close encounter with Mars after 84 Myr, and after 200 Myr there were 5 asteroids encountering Mars, so the resonance is a clear source of Mars crossing asteroids. The first encounter of an asteroid with the Earth happened at approximately 100 Myr. Six asteroids in the simulation, most of them with initial $i \gtrsim 11°$, ended by colliding with the Sun shortly after being captured into the 3:1 resonance with Jupiter (the most common situation), or in the 4:1 resonance with Jupiter, or evolving near the ν_6 secular resonance.

Other MMRs very close to the 1:2M resonance are listed in Table 3. These resonances have much lower strengths, however, for higher values of e they grow in relevance and can compete with the 1:2M resonance, allowing a diffusion in a. We have also found captures in three body mean motion

Resonance	a[AU]	strength ($e = 0.15$)	strength ($e = 0.25$)
$19\lambda_J - 6\lambda$	2.4116	4×10^{-7}	1×10^{-4}
$-4\lambda_E + 15\lambda$	2.4137	6×10^{-6}	5×10^{-3}
$-\lambda_M + 2\lambda$	2.4184	1	1
$22\lambda_J - 7\lambda$	2.4237	2×10^{-8}	1×10^{-5}
$-5\lambda_E + 19\lambda$	2.4351	1×10^{-6}	6×10^{-4}

Table 3: The strongest two body mean motion resonances near $a \sim 2.418$. The resonance strength was calculated following Gallardo (2006) and is given in units relative to the 1:2M resonance strength for two different values of the orbital eccentricity and for fixed $i = 5^\circ$ and $\omega = 60^\circ$. Note the increasing strength of the resonances relative to 1:2M for the more eccentric orbits.

resonances (Nesvorný and Morbidelli, 1998), as for example the $3n_M + n_N - 6n = 0$ resonance at $a \simeq 2.4125$, that involves the mean motions of Mars and Neptune. All these MMRs contribute to the chaotic diffusion observed at high eccentricities.

3. Orbital migration by the Yarkovsky effect

All the results presented up to this point were obtained in the framework of pure gravitational interaction between the asteroids and the planets. It is known (Bottke et al., 2000) that the Yarkovsky effect generates a small extra acceleration due to the natural delay of thermal emission by the asteroid surface, and this effect could significantly modify the capture mechanisms, especially for asteroids with diameter $\lesssim 10$ km.

We found that 80% of the 4022 asteroids located in the 1:2M resonance region have absolute magnitudes $14.9 < H < 17.8$, which corresponds to diameters between $\sim 0.6 - 6.0$ km depending on the geometrical albedo considered. So, we are dealing with a population of asteroids for which the Yarkovsky effect cannot be neglected. This effect can be reproduced with a simplified model by adding a term to the asteroid's acceleration of the form (Roig et al., 2007):

$$\ddot{\vec{r}} = \frac{GM_\odot \dot{a}}{2a^2} \frac{\vec{v}}{v^2} \tag{1}$$

where G is the gravitational constant, $M_\odot$ the solar mass, a the osculating semimajor axis of the asteroid, $\vec{r}$ and $\vec{v}$ are its heliocentric position and velocity, respectively, and $\dot{a}$ the assumed Yarkovsky drift in a that depends on several factors like diameter, rotational axis obliquity, rotational period,

and surface thermal conductivity, K. According to Bottke et al. (2000; 2006), $\dot{a}$ runs from $\sim 10^{-2}$ to $\sim 10^{-5}$ AU/Myr for asteroids with radius from some meters to a few kilometers and values of K between 0.01 and 0.001. The most common variant is the Yarkovsky "diurnal" effect, that makes asteroids with prograde rotation to have $\dot{a} > 0$, and those with retrograde rotation to have $\dot{a} < 0$. In very particular cases, like asteroids with iron-rich surfaces and high values of the thermal conductivity, another variant known as the Yarkovsky "seasonal" effect (that we will not consider here) predominates and produces a secular negative drift in a (Bottke et al., 2006).

We have performed a series of four simulations with four different assumed values of $\dot{a}$: 10^{-2}, 10^{-3}, 10^{-4} and 10^{-5} AU/Myr (hereafter referred as simulations #1, #2, #3 and #4, respectively, see Table 4). In each simulation, we consider two fictitious population of 200 test particles initially located at both sides of the resonance and with values of (e, i) taken from the real population. In order to force the particles to fall into the resonance, we assumed $\dot{a} > 0$ (i.e, prograde rotation) for the particles starting from "the left side" of the resonance, and $\dot{a} < 0$ (i.e., retrograde rotation) for the particles starting from "the right side". This allows us to detect any difference between left and right side populations regarding the capture into the resonance. In these simulations, we do not consider the abrupt and stochastic changes in $\dot{a}$ due to eventual reorientation of spin axes related to non catastrophic collisions. We also ignore the obliquity and rotation rate evolution due to the YORP effect (Vokrouhlický and Čapek, 2002). It must be noted that the simplified model used to simulate the Yarkovsky effect generates a spurious variation in the particles eccentricity, but this is negligible in magnitude. Indeed, if we calculate the total variation in e induced by the Eq, (1) during our simulations only by means of the Gauss planetary equations, we obtain $\sim 10^{-4} - 10^{-3}$ which is small enough to not alter our conclusions.

The simulations spanned a time scale long enough for the total drift in a to be larger than the resonance width (i.e., the asteroids would completely cross the resonance during the simulations provided that no captures occur). We also estimated the time scale of the collisional/gravitational lifetime, $t_{\rm ejec}$, as the time necessary to eject an asteroid from the resonance due to collisions with other asteroids, or due to gravitational perturbations by close encounter with massive asteroids. To compute $t_{\rm ejec}$, we simulated collisions using a Monte Carlo method. We assumed a typical power law population of projectiles (Farinella et al., 1998) with randomly oriented encounter velocities, v_e, taken from a Maxwellian distribution with mean 5.3 km/s. We

Simulation	$\dot{a}$ [AU/Myr]	R [m]	ΔT [Myr]	Δa [AU]	$t_{\rm ejec}$ [Myr]
#1	0.01	1	2	0.02	5 C
#2	0.001	30	20	0.02	10 C
#3	0.0001	600	200	0.02	90 C
#4	0.00001	5000	1000	0.01	1000 E

Table 4: Parameters of four simulations using different Yarkovsky drifts $\dot{a}$. Each simulation was composed of two fictitious populations of 200 bodies. Each population was initially located at each side of the resonance. The typical radius of the bodies, R, was estimated according to Bottke et al. (2006) and assuming a thermal conductivity between 0.01 and 0.001. Table gives the total time span, ΔT, of the simulations and the equivalent total drift, Δa. The ejection timescale, $t_{\rm ejec}$, has a large uncertainty and it was estimated as the mean time necessary for the particles to be ejected from the resonance due to either gravitational perturbations by close encounters with massive asteroids (labeled as "E"), or collisions with other asteroids, including disruption events (labeled as "C").

also assumed an impulse $\delta v = (R_{\rm proj}/R_{\rm target})^3 v_e$, and computed δa via Gauss planetary equations, considering disruption events as in Bottke et al. (2005).

Gravitational perturbations by massive asteroids (Nesvorný et al., 2002) were also estimated via Gauss planetary equations, using a Monte Carlo method to calculate the impulse $\delta v = 2mGv_e(G^2(M+m)^2 + \rho^2 v_e^4)^{-1/2}$ due to hyperbolic encounters with the 10 most massive asteroids, where ρ is the randomly chosen impact parameter, M the mass of the target assuming a density of 2.7 g/cc, and m the mass of any of the randomly chosen massive asteroids. The mean time interval between encounters with the 10 most massive asteroids and with impact parameter $\rho < 0.01$ AU was taken to be 15,600 yr. This time scale was deduced from the intrinsic collision probability of 2.86×10^{-18} km^{-2}yr^{-1}, typical for the inner region of the Main Belt.

The gravitational perturbations by massive asteroids are approximately the same for all the range of asteroid sizes. On the other hand, the effect of collisions is only relevant for smaller asteroids. In our simulations, we found that $t_{\rm ejec}$ is determined by collisions for asteroids with $R \lesssim 2.5$ km and by close encounters with the massive asteroids otherwise. These close encounters drop off the half-life obtained from Fig. 8 to ~ 1 Gyr.

3.1. Capture in resonance and chaotic diffusion

The analysis of the time evolution of the semimajor axis shows that the main mechanism that keeps the asteroid fixed in a is the resonance stickiness. Figure 10 shows a typical example of a particle from the "left side"

group in simulation #4. The Yarkovsky effect generates a positive drift in semimajor axis up to $t \simeq 500$ Myr, when the particle gets sticked to the resonance alternating between the "left" and "right" sides. At $t \simeq 750$ Myr, the particle gets captured into the resonance, and after that it evolves switching between sticking and getting inside the resonance. It is worth noting that after $t \simeq 500$ Myr the drift in a stopped, and a new dynamical mechanism drives the eccentricity. This mechanism partially erases the "memory" of the particle, mainly its proper eccentricity but also its proper inclination. Captures from the "right side" exhibit a similar behavior. In some cases, the particle is neither captured into the resonance nor in a sticky orbit, and in these cases the eccentricity is not altered. This is illustrated from the results of simulation #4 shown in Figs. 11 and 12. Figure 11 shows the population evolving from the "right side" in the (a_m, e_m) plane, and Fig. 12 shows the population evolving from the "left side" in the (e_m, i_m) plane; the diffusion in this later case is significant for asteroids captured into resonance and negligible for asteroids that quickly escape from the resonance.

Calculating the a_m of each particle in a 1 Myr running window, we computed the number of asteroids inside the resonance or sticked to the resonance as a function of time. We also computed the time $t_{\rm res}$ that each asteroid remains captured into/sticked to the resonance. We considered the asteroid was captured/sticked when a_m falls inside the resonance region in the (a_m, e_m) space defined in Fig. 4. Analyzing all four simulations, we found that the total effect on the eccentricity when evolving inside the resonance is somehow proportional to the magnitude of the Yarkovsky effect and to the time the particle remained captured into the resonance (Fig. 13). The diffusion in mean eccentricity, Δe_m, as a function of the lifetime in the resonance $t_{\rm res}$, in Myr, can be approximately described by

$$\Delta e_m \sim 6\, \dot{a}\, t_{\rm res}^{\beta} \tag{2}$$

where $\dot{a}$ is in AU/Myr and β is 0.54, 0.75 and 1.07 for simulations #2, #3 and #4, respectively. The value of Δe_m deduced from this expression is only an indication of the actual value, considering the large spread of the data observed in Fig. 13. From this figure, we can conclude that, in general, the largest diffusion in eccentricity corresponds to simulation #4, i.e., to the largest asteroids.

Simplified analytical models (see for example Murray and Dermott, 1999) predict that captures from "approaching" orbits (i.e., asteroids migrating

towards Mars, or equivalently, from the "right side" population) are more successful than captures from "receding" orbits (i.e., from the "left side" population), but in our simulations we did not find any significant difference between the two populations regarding the probability of capture. As an example, Fig. 14 shows the fraction of asteroids captured into resonance as a function of the time in simulation #3 (i.e., for a Yarkovsky effect corresponding to an asteroid size of some hundred meters), distinguishing between the left and right populations. The same behavior was obtained in all the four simulations, but in different time scales.

Using the values of $t_{\rm res}$ computed for all particles in all the four simulations, we determined the cumulative distribution of the *scaled* lifetime in the resonance, $L = t_{\rm res}/T$, where T is the time that would be necessary to cross the resonance region due to the Yarkovsky drift in a only (i.e., assuming that no captures occur). The result is shown in Fig. 15. If $L < 1$ in all the simulations, the distribution of the asteroid semimajor axes would show a gap or a depression at the resonance location. On the other hand, asteroids with $L > 1$ would be the ones contributing to the total excess of asteroids inside the resonance. Looking at the left part of Fig. 15 ($L < 1$), it is evident that the smaller the asteroids the larger the scaled lifetime, therefore, an excess of small asteroids inside the resonance with respect to the background should be expected. This is consistent with our analysis of the size distributions (Section 2.2 and Fig. 7). It is worth mentioning that Tsiganis et al. (2003) also found an excess of small asteroids in the 7:3 resonance with Jupiter due to a selective dynamical process generated by the Yarkovsky effect.

The higher capture probability at larger eccentricities, and the diffusive process in eccentricity inside the resonance, explain the different eccentricity distributions observed in the resonant population compared to the non resonant background population.

3.2. V-type asteroids as tracers

V-type asteroids have unique surface colors, and they are considered to be members of a dynamical family formed as a result of an impact on Vesta's surface. There are several V-type asteroids far from the domain of the Vesta dynamical family in the space of proper elements, a fact that has challenged the understanding of the dynamical link between these asteroids and the Vesta family (Nesvorný et al., 2008).

Roig and Gil-Hutton (2006), at their Table 2, provide a list of candidate V-type asteroids that were not identified as members of the Vesta dynamical

Asteroid	a_p[AU]	e_p	i_p[°]	H	σ_c[°]	$\Delta\sigma$[°]
(3331) Kvistaberg	2.41875	0.114	3.58	13.2	160	360
(5599) 1991 SG1	2.41869	0.155	7.23	12.5	175	360
(12027) 1997 AB5	2.41840	0.174	6.22	14.6	183	287
(40733) 1999 SM17	2.41846	0.113	6.80	15.0	167	340
(68064) 2000 YU67	2.41893	0.152	7.13	15.2	179	360
(122441) 2000 QH126	2.41837	0.100	6.92	15.4	177	279
(109721) 2001 RE54	2.41848	0.051	3.93	16.0	217	180
(2798) Vergilius	2.41848	0.044	5.94	13.1	214	200
(32366) 2000 QA142	2.41840	0.213	6.31	13.9	158	292

Table 5: Resonant V-type asteroids not identified as members of Vesta dynamical family. The first seven ones are from Roig and Gil-Hutton (2006). a_p, e_p and i_p are the proper semimajor axes, eccentricities and inclinations, respectibely, H is the absolute magnitude, and σ_c and $\Delta\sigma$ are the libration center and libration amplitude, respectively.

family. From that list, we identified seven asteroids evolving in the 1:2M resonance, whose dynamical parameters are shown in Table 5. These asteroids are very close to the region of the Vesta dynamical family, so they could have evolved in e_p due to the diffusive process inside the resonance, masking their dynamical origin as Vesta family members. The only exceptions are probably (3331) Kvistaberg and (109721) 2001 RE54, because their i_p could not be explained by a diffusive process inside the resonance according to our numerical studies (see for example Fig. 9).

Looking at the photometric data from the SDSS, we identified other two candidate V-type asteroids among the resonant population: (32366) 2000 QA142 and (2798) Vergilius. The orbital evolution of these two asteroids, together with (12027) 1997 AB5, are shown in Fig. 16. The low eccentricity of (2798) and the high eccentricity of (12027) are both compatible with the diffusive processes inside the resonance.

The case of (32366) is a very special one, because its e_p is larger by approximately 0.1 with respect to the value of e_p expected for the V-type asteroids. Assuming a geometric albedo of $\sim 0.3 - 0.4$, typical of V-types, the diameter of asteroid (32366) is $\sim 3.5 - 4.0$ km. This size is consistent with a drift rate $|\dot{a}| \approx 1.25 - 1.43 \times 10^{-5}$ AU/Myr (Roig et al., 2007), so we can apply Eq. (2) or look at Fig. 13 to conclude that the necessary timescale of resonant evolution to increase the eccentricity by 0.1 is approximately 800 Myr. In fact, Fig. 16 shows that this asteroid has important excursions in

(e_m, i_m); thus, it could have obtained its present eccentricity after several hundred millon years of resonant evolution.

4. Discussion and Conclusions

Our analysis of the size distribution of the real asteroids in the region of the 1:2M resonance has confirmed a significant lack of low H asteroids in the resonant population compared to the non resonant one. This result is consistent with the ratio of small to big asteroids inside and outside the resonance that we obtained from our simulations of fictitious asteroids, using different values of the drift in a induced by the Yarkovsky effect according to different asteroid sizes. It is worth mentioning that pure gravitational processes, like chaotic diffusion, do not distinguish between asteroid sizes; therefore in the absence of the Yarkovsky effect the size distribution in the resonant population should be the same as in the non resonant population.

The diffusion in (e_m, i_m) generates misidentification of resonant asteroids belonging to the Vesta and Nysa-Polana families, whose proper elements differ from the nominal values of the families. The Massalia dynamical family is less affected by the resonance, probably due to the low proper inclination of its members that protects them from large diffusion in eccentricity and inclination. Vokrouhlický et al. (2006) modeled the orbital evolution of Massalia family members and found that 16% of the members that cross the 1:2M resonance are misidentified due to the effect of the resonance. This is in good agreement with our result from Table 2, indicating that inside the resonance about 11% of the Massalia family members would not be detected as such.

When the resonant asteroids reach the chaotic region at $e_m > 0.22$, they escape from the resonance mostly by diffusion in a. A small fraction remains captured at higher eccentricities, but because of their large amplitude of σ they undergo encounters with Mars and escape from the resonance too. Escapes by reaching the secular resonance ν_6 were also observed. For the small asteroids, the escape by diffusion in a is the rule, but for the big ones it first operates a diffusion in eccentricity, until they reach $e_m > 0.22$, and then operates the diffusion in a. A fraction of approximately 6% of the long lived asteroids end by colliding with the Sun, mainly after reaching the 3:1 resonance with Jupiter. Asteroids that tend to follow this path are the ones with the higher inclinations.

Campins et al. (2010) discussed the origin of the NEA (101955) 1999 RQ36, with a diameter of 580 m, and concluded that it comes from the Polana branch of the Nysa-Polana complex, by reaching the ν_6 resonance due to the Yarkovsky effect over long timescales. According to our results, we suggest another possible path to transfer asteroids from the Polana region to a NEA orbit: over a small timescale, an asteroid could reach the 1:2M resonance, excite its eccentricity by diffusion while evolving in resonant motion, and finally reach the ν_6 or the 3:1 resonances on a much shorter timescale than the one proposed by Campins et al. (2010), because for higher eccentricities the diffusion in semimajor axis is faster, and the secular resonance ν_6 is closer to the Polana branch.

The mean lifetime in the resonance of the largest members of the resonant population, i.e., those not affected by the Yarkovsky effect, is quite long. These objects can stay evolving in the resonance over timescales of 1 Gyr, even considering the effects of collisions with other asteroids and/or ejections due to close encounters with massive asteroids. This must leave some signature in the orbits of asteroids with diameters larger than 10 km, because after 1 Gyr of resonant evolution, the change in eccentricity should be of the order of $\sim 0.04 - 0.15$ (Fig. 9). On the other hand, small resonant asteroids should have been captured in more recent times.

The negligible effect of the Yarkovsky drift on a large asteroid like (142) Polana raises the problem of the origin of its present orbit. There is an analogue case in the resonance 7:3 with Jupiter: asteroid (677) Aaltje (Tsiganis et al., 2003). One possible mechanism to explain such cases would be chaotic diffusion enhanced by close encounters with massive asteroids which, over Gyr timescales, might push the big asteroids into the resonance. A more efficient alternative, although not yet proved to be compatible with the dynamical history of Mars, would be a slow migration of Mars orbit. This later mechanism of capture is dynamically possible, as we have checked with some numerical experiments, but it does not distinguish between asteroid sizes.

The existence of different H distributions in the resonant and non resonant populations, with an excess of small asteroids inside the resonance compared to the background, is an indication that the main mechanism that replenishes the resonance at present is the Yarkovsky effect, rather than either chaotic diffusion, close encounters with massive asteroids, or Mars orbital migration.

Acknowledgments

We are grateful to E. Falco for the support provided at the earlier stages of the numerical integrations, and to M. Cañada by their analysis of the SDSS data. We acknowledge the criticism and suggestions given by M. Brož and another anonymous reviewer, that contributed to improve this work. This study was developed with partial support by PEDECIBA, and in the framework of the project "Caracterización de las Poblaciones de Cuerpos Menores del Sistema Solar" (ANII FCE 2007 318). F.R. acknowledges support by CNPq.

Appendix: the excess of small asteroids in the resonance

We have defined $L = t_{\rm res}/T$, where T is the time that would be necessary to cross the resonance region due to the Yarkovsky drift in a only. Taking a mean width for the resonance of 0.004 AU we have $T = 0.004\,{\rm AU}/\dot{a}$. In steady state, the number of resonant asteroids, n, is

$$n = \dot{N} < t_{\rm res} > \tag{3}$$

where

$$\dot{N} = \frac{dN}{da}\,\dot{a} \tag{4}$$

is the injection's rate of asteroids into the resonance and $< t_{\rm res} >$ the mean lifetime in resonance, both depending on the asteroid size. By definition of L we have $< t_{\rm res} >=< L > T$ for each of the four simulations. Now, taking into account Eqs. 3 and 4 and the definition of T, we can calculate the ratio n_s/n_l between small and large asteroids inside the resonance

$$\frac{n_s}{n_l} = \frac{dN_s}{dN_l}\frac{< L_s >}{< L_l >} \tag{5}$$

where dN_s/dN_l is the ratio outside the resonance. The behavior of L as seen in Fig. 15 is not very different for the four simulations at the right part of the plot, corresponding to long lived resonant asteroids. But, looking at the left part of the plot ($L < 1$) it is evident that $L_s/L_l > 1$ then, an excess of small asteroids inside the resonance with respect to outside is expected.

References

Bottke, W.F, Rubincam, D.P, Burns, J.A, 2000. Dynamical evolution of main belt meteoroids: Numerical simulations incorporating planetary perturbations and Yarkovsky thermal forces. Icarus 145, 301-331.

Bottke, W.F., Durda, D.D., Nesvorný, D., Jedicke, R., Morbidelli, A., Vokrouhlický, D., Levison, H., 2005. The fossilized size distribution of the main asteroid belt. Icarus 175, 111-140.

Bottke, W.F, Vokrouhlický, D., Rubincam, D.P, Nesvorný, D., 2006. Annu. Rev. Earth Planet. Sci. 34, 157-191.

Campins, H., Morbidelli, A., Tsiganis, T., de León, J., Licandro, J., Lauretta, D., 2010. The origin of asteroid 101955 (1999 RQ36). ApJL, 721, L53-L57.

Carruba, V., Michtchenko, T.A., 2009. A frequency approach to identifying asteroid families. II. Families interacting with nonlinear secular resonances and low-order mean-motion resonances. Astronomy and Astrophysics, Volume 493, Issue 1, pp.267-282.

Cellino, A., Zappalà, V., Doressoundiram, A., Di Martino, M., Bendjoya, Ph., Dotto, E., Migliorini, F. , 2001. The Puzzling Case of the Nysa-Polana Family. Icarus 152, 225-237.

Farinella, P., Vokrouhlický, D. and Hartmann, W. K., 1998. Meteorite Delivery via Yarkovsky Orbital Drift. Icarus 132, 378-387.

Fernández, J.A., Gallardo, T., Brunini, A., 2002. Are There Many Inactive Jupiter-Family Comets among the Near-Earth Asteroid Population?. Icarus 159, 358-368.

Gallardo, T., 2006. Atlas of the mean motion resonances in the Solar System. Icarus 184, 29-38.

Gallardo, T., 2007. The Mars 1:2 resonant population. Icarus 190, 280-282.

Gallardo, T., 2009. A New Dynamical Population of Asteroids. RMAA Conf. Series vol. 35, 21-22.

Gallardo, T., Ferraz-Mello, S., 1997. Understanding librations via time-frequency analysis. Astron. J. 113, 863-870.

Malishkin, L., Tremaine, S., 1999. The Keplerian Map for the Planar Restricted Three-Body Problem as a Model of Comet Evolution. Icarus 141, 341-353.

Morbidelli, A., Nesvorný, D., 1999. Numerous Weak Resonances Drive Asteroids toward Terrestrial Planets Orbits. Icarus 139, 295-308.

Morbidelli, A., Zappalà, V., Moons, M., Cellino, A., Gonczi, R., 1995. Asteroid Families Close to Mean Motion Resonances: Dynamical Effects and Physical Implications. Icarus 118, 132-154.

Mothé-Diniz, T., Roig, F., Carvano, J.M., 2005. Reanalysis of asteroid families structure through visible spectroscopy. Icarus 174, 54-80.

Murray, C. D., Dermott, S. F., 1999. Solar System Dynamics, Cambridge University Press.

Nesvorný, D., Morbidelli, A., 1998. Three-Body Mean Motion Resonances And The Chaotic Structure Of The Asteroid Belt. Astron. J. 116, 3029-3037.

Nesvorný, D., Morbidelli, A., Vokrouhlický, D., Bottke, W. F., and Brož, M., 2002. The Flora Family: A Case of the Dynamically Dispersed Collisional Swarm?. Icarus 157, 155-172.

Nesvorný, D., Roig, F., Gladman, B., Lazzaro, D., Carruba, V., Mothé-Diniz, T., 2008. Fugitives from the Vesta family. Icarus 193, 85-95.

Press W. H., Teukolsky, S. A., Vetterling, W. T., Flannery, B. P., 1997. Numerical Recipes in Fortran 77: The Art Of Scientific Computing, p. 617, Cambridge University Press.

Roig, F., Gil-Hutton, R., 2006. Selecting candidate V-type asteroids from the analysis of the Sloan Digital Sky Survey colors. Icarus 183, 411-419.

Roig, F., Nesvorný, D., Gil-Hutton, R., Lazzaro, D., 2007. V-type asteroids in the middle main belt. Icarus 194, 125-136.

Tsiganis, K., Varvoglis, H., Morbidelli, A., 2003. Short-lived asteroids in the 7/3 Kirkwood gap and their relationship to the Koronis and Eos families. Icarus 166, 131-140.

Vokrouhlický D., Čapek, D., 2002. YORP-induced long term evolution of the spin rate of small asteroids and meteoroids: Rubincam's approximation. Icarus 159, 449-467.

Vokrouhlický D., Brož, M., Bottke, W. F., Nesvorný, D., Morbidelli, A., 2006. Yarkovsky/YORP chronology of asteroid families. Icarus 182, 118-142.

Zappalà, V., Bendjoya, P., Cellino, A., Farinella, P., Froeschlé, C., 1995. Asteroid families: search of a 12487-asteroid sample using two different clustering techniques. Icarus 116, 291-314.

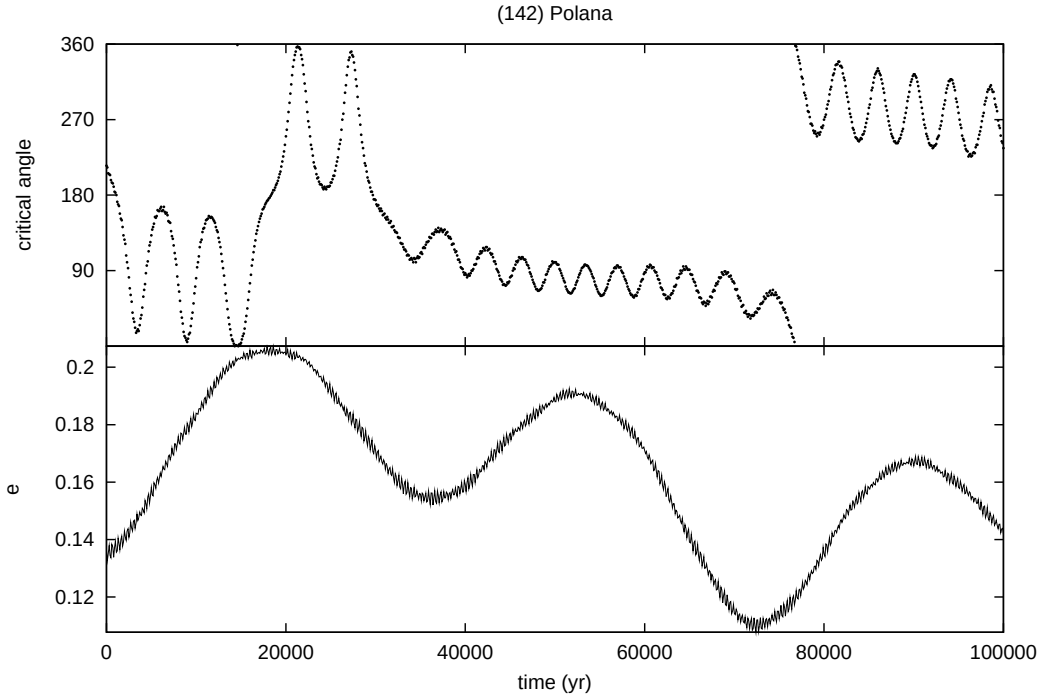

Figure 1: Asymmetric librations of the critical angle $\sigma = 2\lambda - \lambda_M - \varpi$ of (142) Polana, switching its libration center at $t \backsimeq 19.000$, 30.000 and 77.000 yr. The eccentricity variations are due to the secular forced modes.

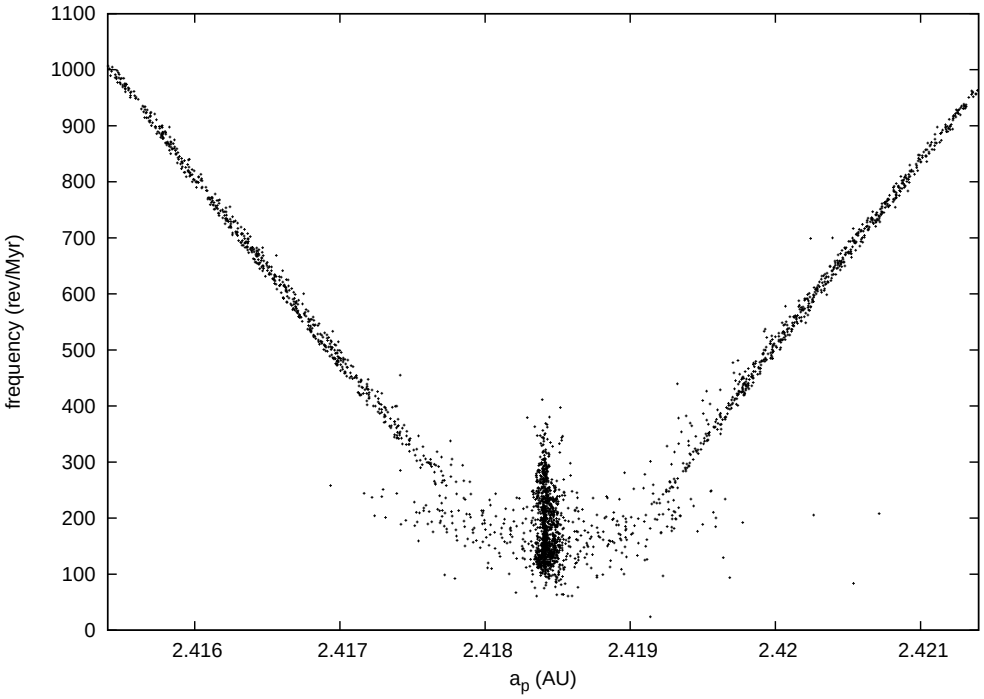

Figure 2: Frequency *vs.* proper semimajor axis at the end of a numerical simulation of 4022 real asteroids over 30,000 years. Each asteroid is represented by a dot corresponding to its a_p and to the most representative frequency in the time evolution of a. The central concentration at $a_p \simeq 2.4184$ corresponds to librations and horseshoes, the straight lines ($a_p \lesssim 2.4174$ and $a_p \gtrsim 2.4194$) correspond to circulations, and the intermediate zone corresponds to transitions between horseshoes and circulations.

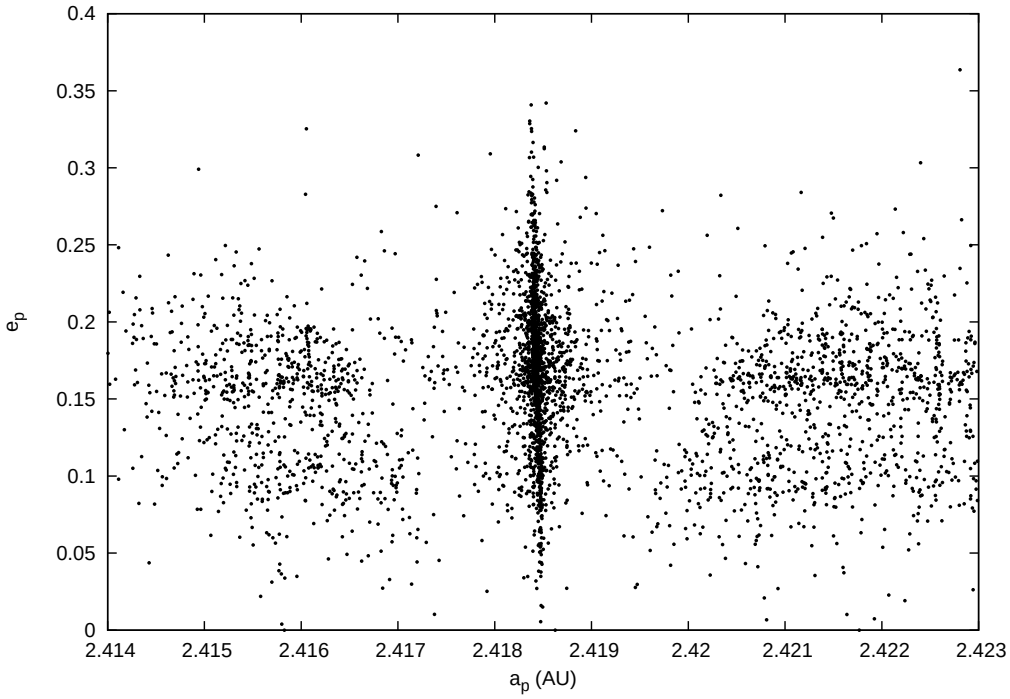

Figure 3: Proper elements obtained from a numerical integration of 4022 real asteroids over 1 Myr. Each asteroid is represented by a dot corresponding to its a_p and e_p. The central region corresponds to librations and horseshoes. The increasing width of the resonance as a function of e_p is evident.

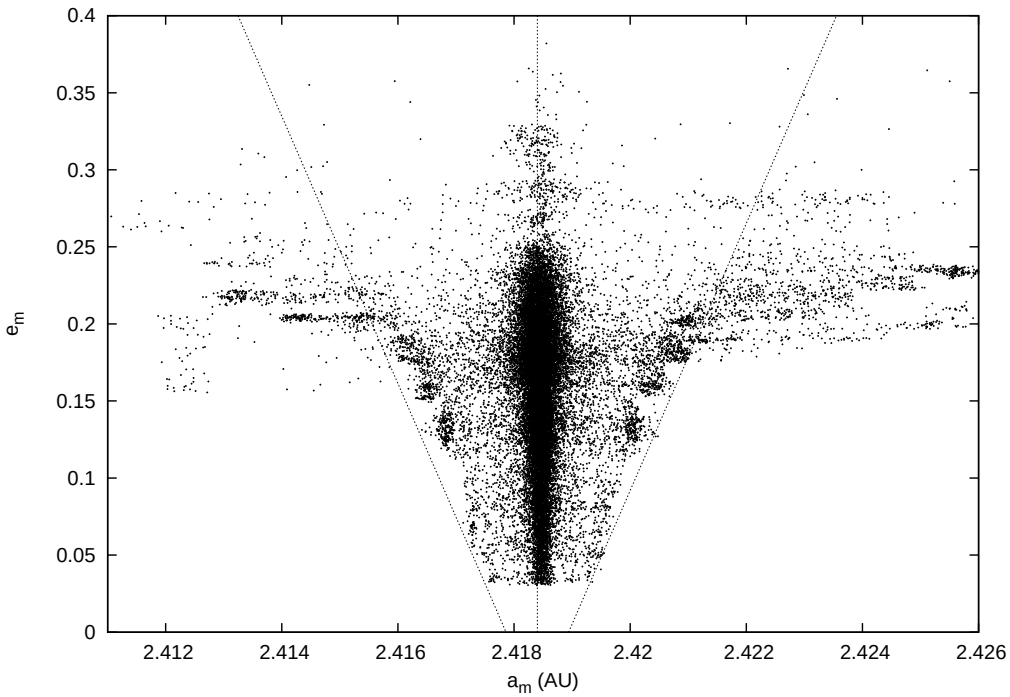

Figure 4: Mean orbital elements, obtained from a 1 Myr running window, of 100 resonant asteroids from the ASTORB database numerically integrated over 1 Gyr. The concentration at $a_m \simeq 2.4184$ AU is due to librations and horseshoes. The concentration at the borders of the resonance is due to the phenomenon of stickiness. The behavior at $e_m > 0.2$ is due to chaotic diffusion dirven by the overlap of several high order resonances. The limits of the resonance are approximately given by the shaded lines. (Low resolution version)

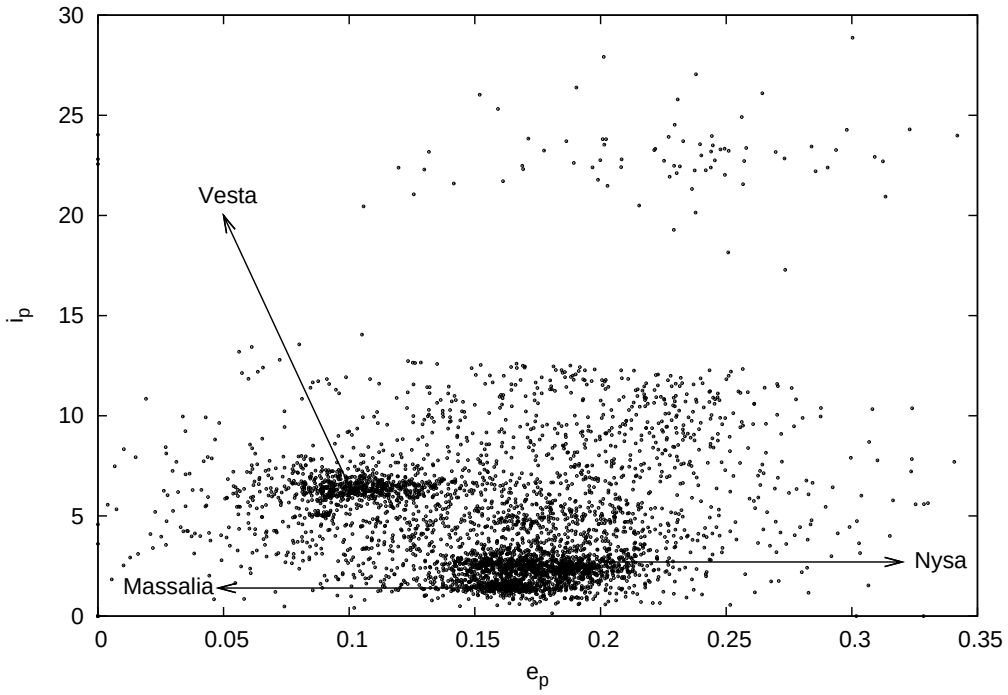

Figure 5: Proper elements of the population of 4022 asteroids inside and close to the resonance. It is possible to identify three clusters that can be associated to the families of Vesta, Nysa-Polana and Massalia. See Table 2 for details. The empty region over $i_p \sim 15^\circ$ is due to the secular resonance ν_6.

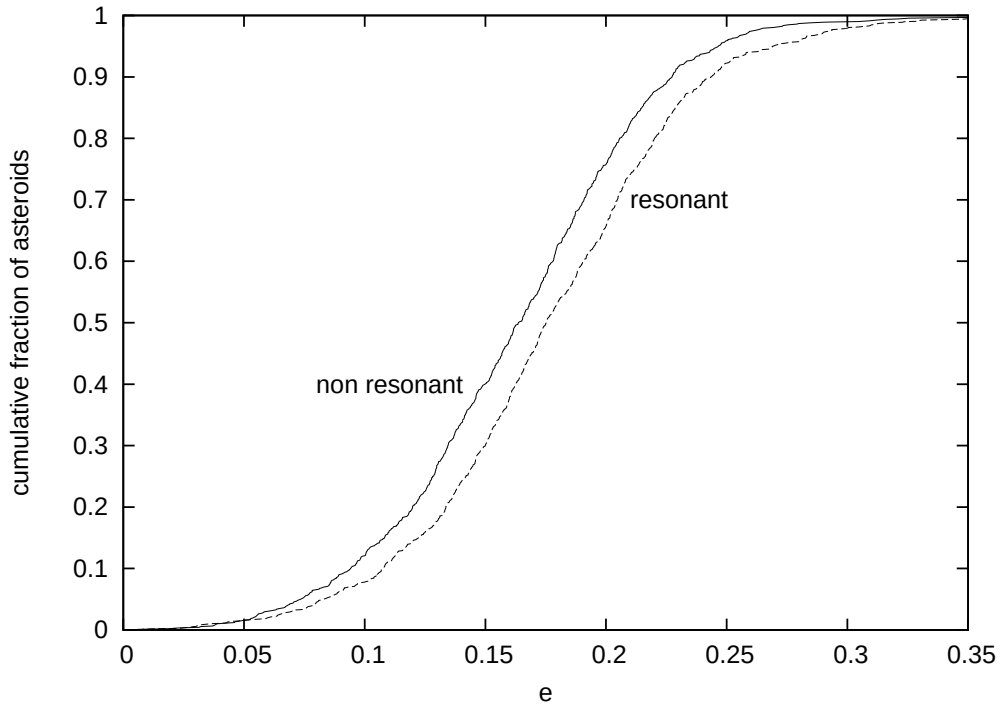

Figure 6: Cumulative distribution of the eccentricities for the resonant and non resonant asteroids. The resonant asteroids have comparatively more eccentric orbits than the non resonant ones.

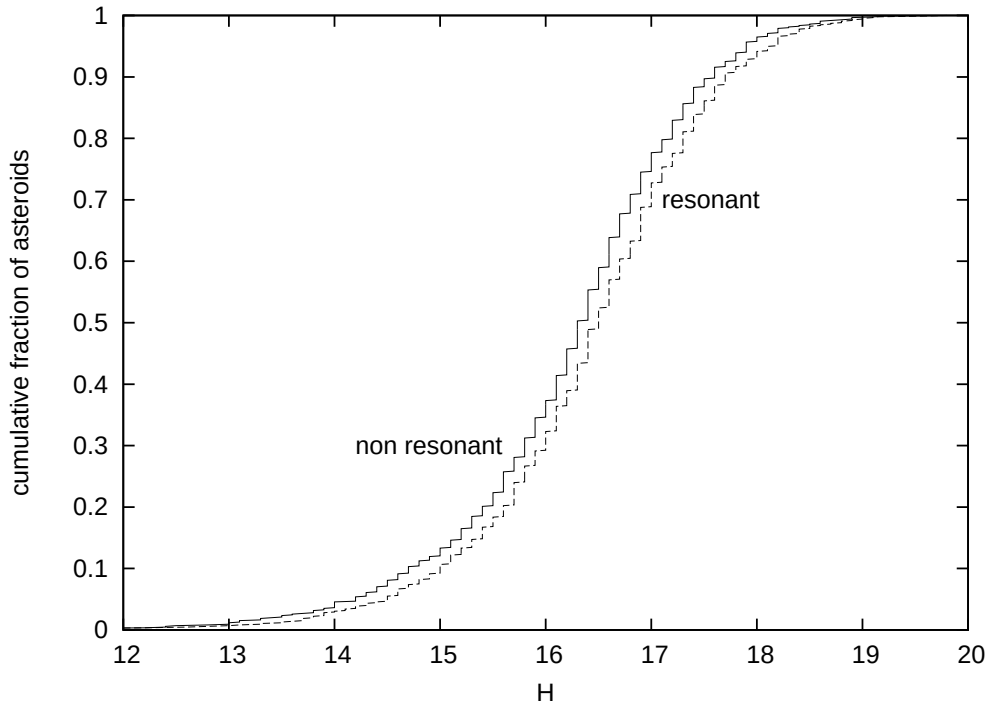

Figure 7: Cumulative distribution of the absolute magnitudes for two unbiased samples of resonant and non resonant asteroids. The two samples of 855 asteroids each, have the same eccentricity distribution in order to avoid possible discovery biases due to different perihelion distances. The resonant asteroids are comparatively smaller than the non resonant ones.

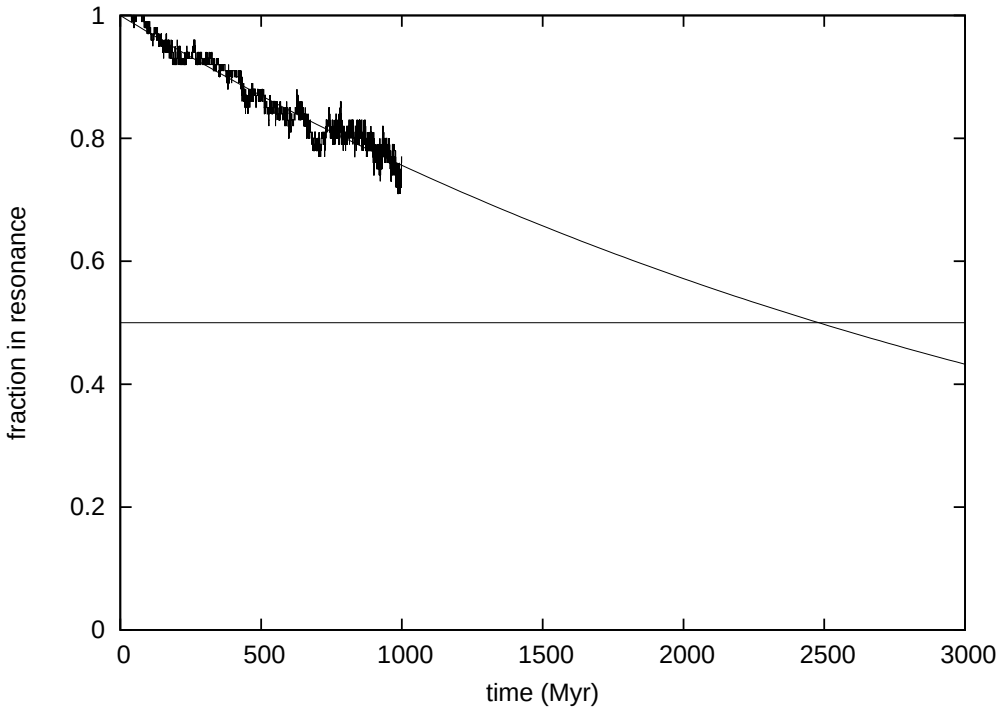

Figure 8: Time decay of the sample of 100 asteroids shown in Fig. 4, initially in resonant motion. A power law fit gives a half-life inside the resonance of 2.5 Gyr.

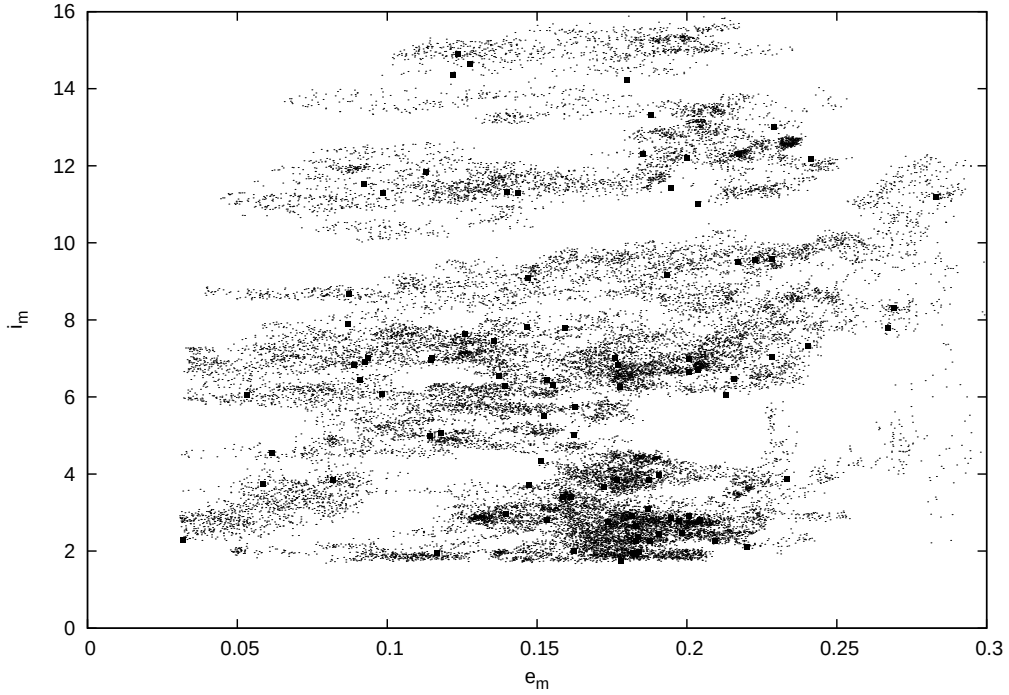

Figure 9: Diffusion in (e_m, i_m) of the sample of 100 asteroids shown in Fig. 4. Diffusion is approximately proportional to the time span of resonant evolution. Squares indicate the initial values of the orbits. (Low resolution version)

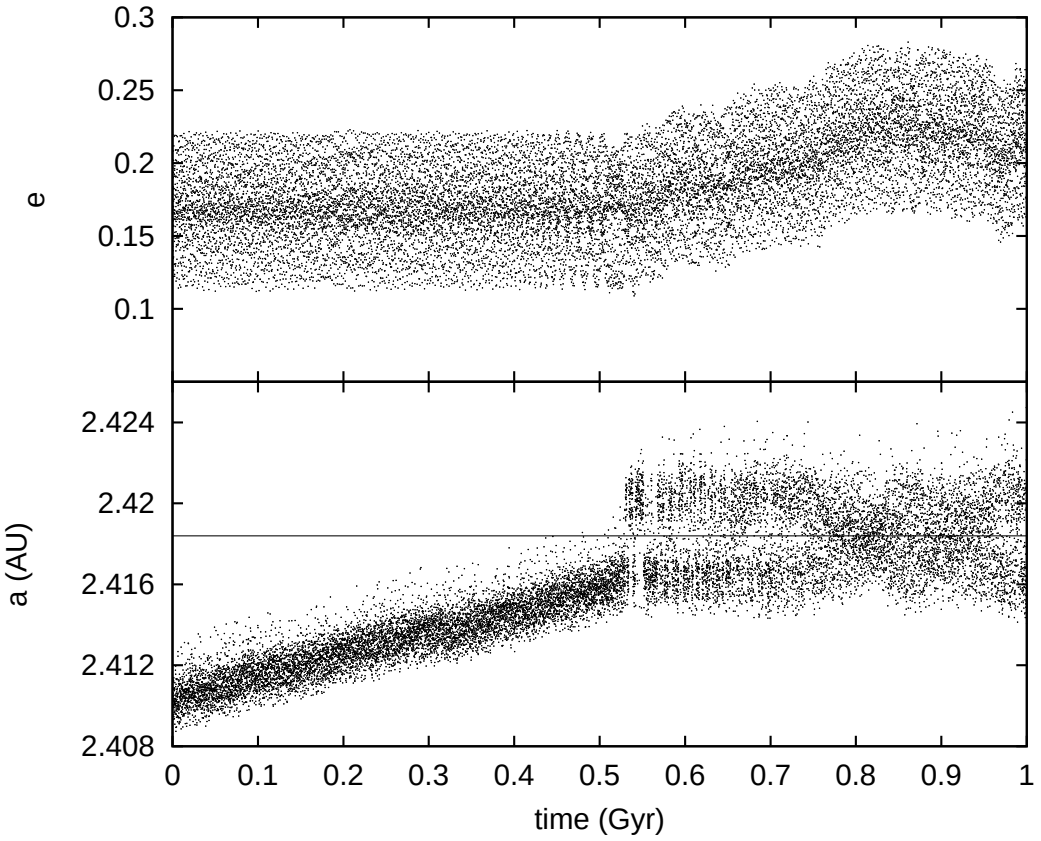

Figure 10: Simulation including a Yarkovsky effect corresponding to a fictitious asteroid with a radius of some kilometers (simulation #4). The asteroid suffers a drift in semimajor axis up to get sticked to the resonance, then starting a diffusive process in e. The exact location of the resonance is indicated with a line.

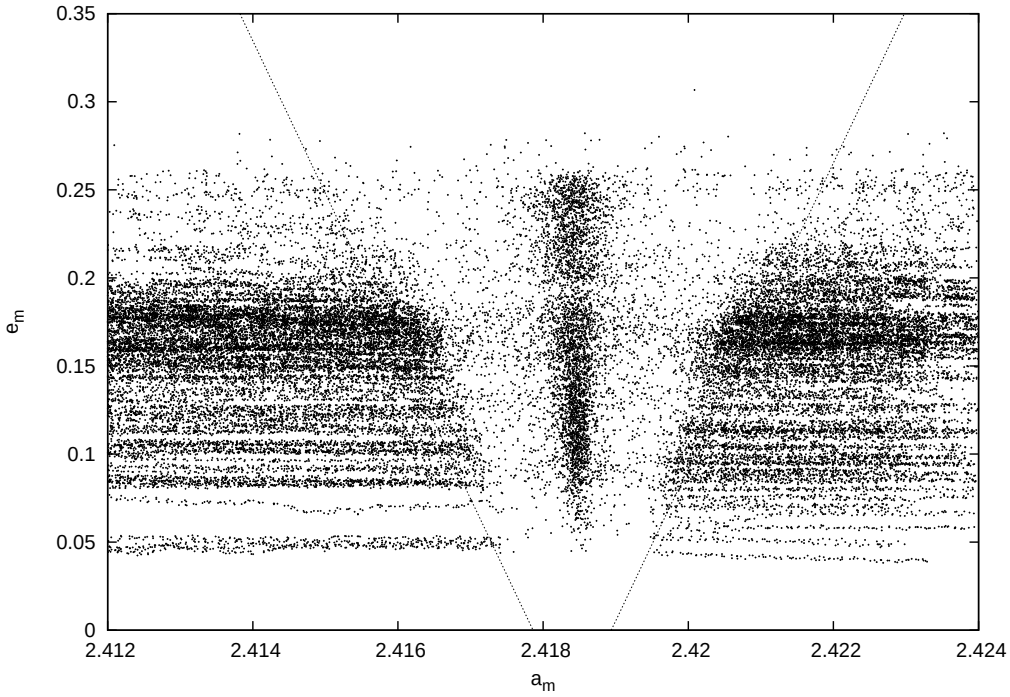

Figure 11: The evolution of the whole population of 200 particles in the simulation with a Yarkovsky effect corresponding to an asteroid with a radius of some kilometers (simulation #4), initially located at the right side of the resonance and with $\dot{a} < 0$. Dotted lines correspond to the limits of the resonance as computed in Fig. 4. (Low resolution version)

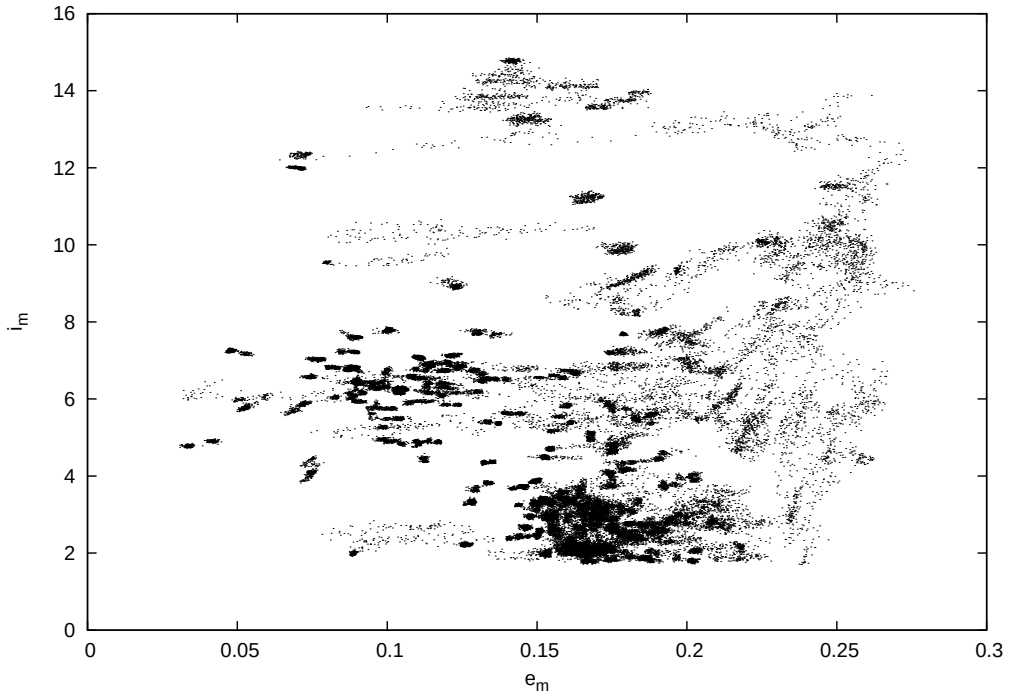

Figure 12: The evolution of the whole population of 200 particles in the simulation with a Yarkovsky effect corresponding to an asteroid with a radius of some kilometers (simulation #4), initially located at the left side of the resonance and with $\dot{a} > 0$. Note the lower diffusion compared to Fig. 9. Particles that remain captured into the resonance over a short period of time, or not captured at all, do not show diffusion in (e_m, i_m). Note also the diffusion in inclination for $e_m > 0.22$. (Low resolution version)

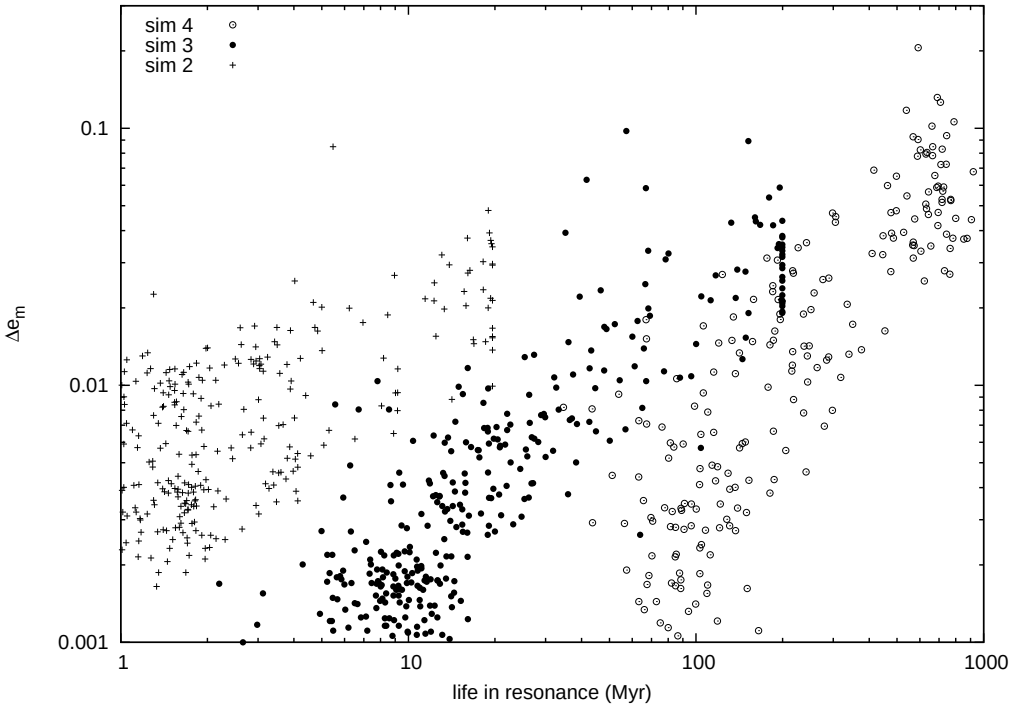

Figure 13: Total variations in e_m as a function of the total lifetime in the resonance, $t_{\rm res}$, for the simulations #2, #3 and #4, starting from both the left and right sides of the resonance. The weaker the Yarkovsky effect, the longer the time evolving in the resonance and the larger the total diffusion in eccentricity. The total diffusion in eccentricity follows an approximate power law with $t_{\rm res}$.

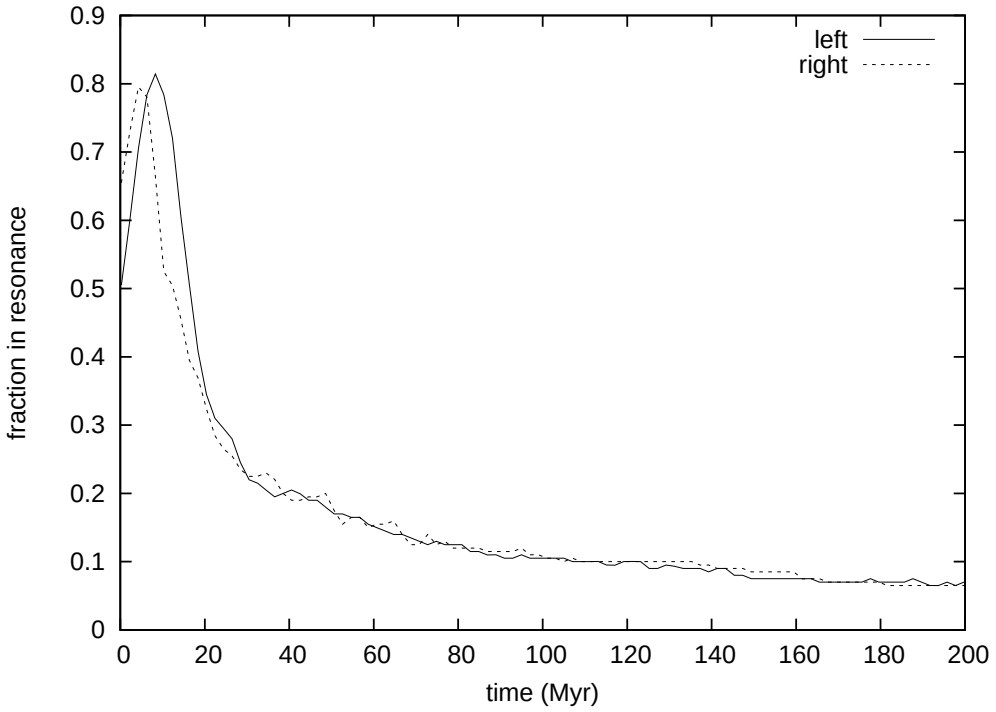

Figure 14: Fraction of the population captured into the resonance, differentiating between the left and right sides populations, in the case of simulation #3 (i.e., with a Yarkovsky effect corresponding to asteroids with radii of some hundreds meters). All the four simulations (see Table 4) show a similar behavior: the evolution from the left and right populations is indistinguishable, and the tails of long lived asteroids in both cases are approximately the same.

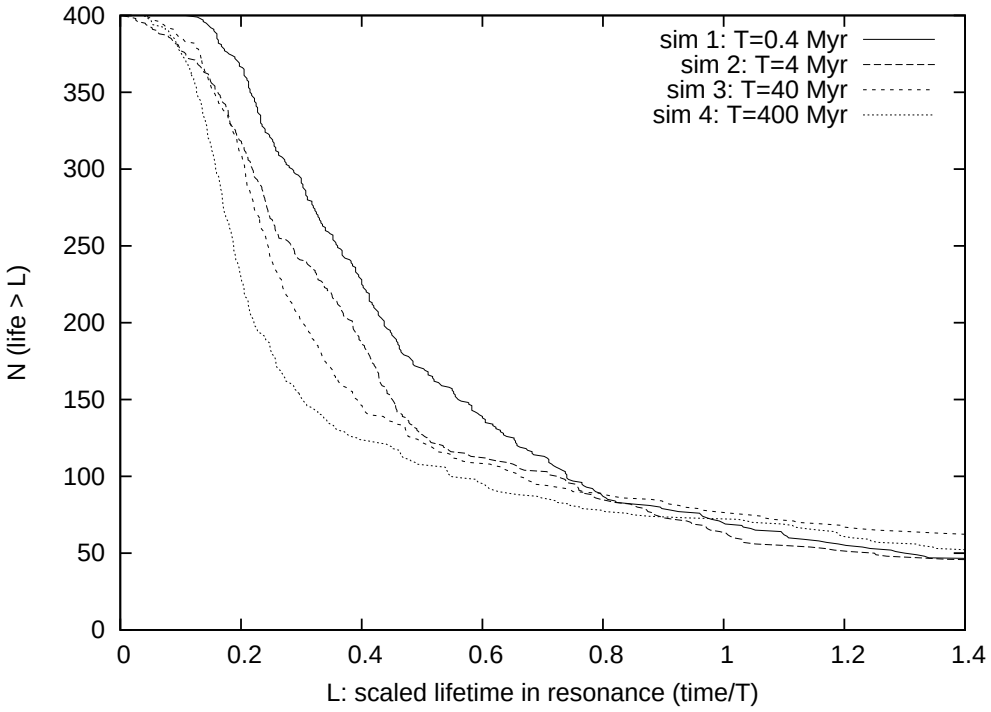

Figure 15: Cumulative distribution of the scaled lifetime in the resonance L for all the simulations with Yarkovsky effect. The left and right populations appear merged. The lifetime in the resonance is scaled according to the time T necessary to drift by 0.004 AU, which is an adopted mean width for the resonance. The decay of the populations is proportional to the Yarkovsky effect, but in the scaled time the decay is approximately similar for all the simulations, especially at the right part of the plot (i.e. long lived asteroids). $L > 1$ corresponds to asteroids that have their migration slowed, on average, by the resonance, whereas $L < 1$ corresponds to asteroids that have their migration accelerated by the resonance.

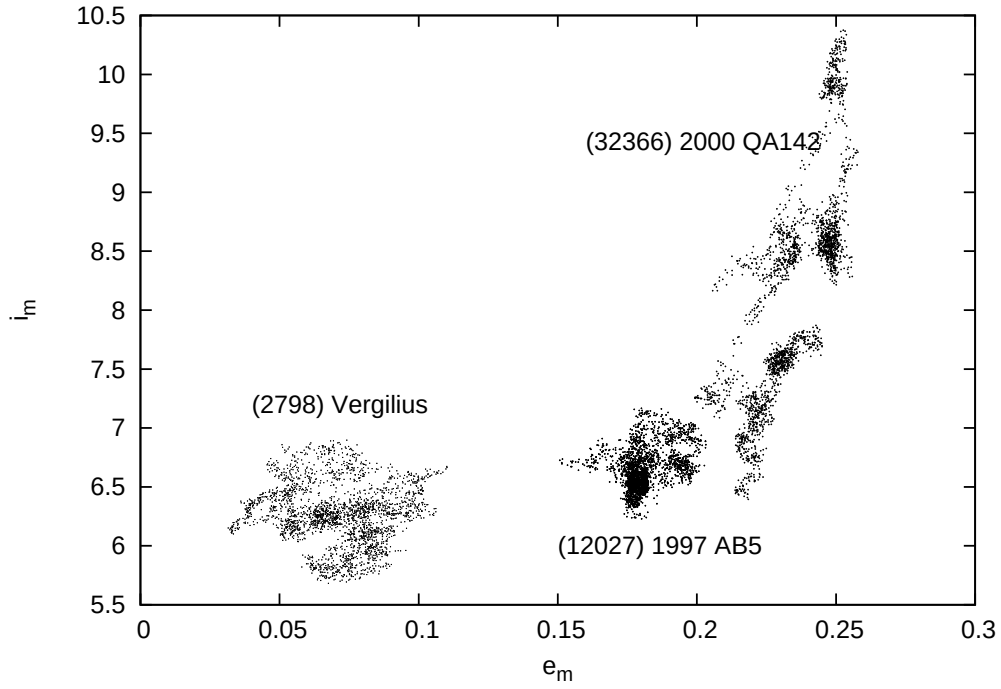

Figure 16: Diffusion over 1 Gyr of three candidate V-type asteroids that evolve inside the 1:2M resonance and were not identified as members of the Vesta dynamical family. These asteroids are included in the sample of 100 asteroids whose evolution is shown in Fig. 9.